



Research paper

Highly selective photocatalytic conversion of CO₂ by water over Ag-loaded SrNb₂O₆ nanorods



Rui Pang^a, Kentaro Teramura^{a,b,*}, Hiroyuki Asakura^{a,b}, Saburo Hosokawa^{a,b},
Tsunehiro Tanaka^{a,b,*}

^a Department of Molecular Engineering, Graduate School of Engineering, Kyoto University, Kyoto 615-8510, Japan

^b Elements Strategy Initiative for Catalysts & Batteries (ESICB), Kyoto University, 1-30 Goryo-Obara, Nishikyo-ku, Kyoto 615-8245, Japan

ARTICLE INFO

Article history:

Received 25 April 2017

Received in revised form 8 June 2017

Accepted 17 June 2017

Available online 24 June 2017

Keywords:

Photocatalytic conversion of CO₂

H₂O

SrNb₂O₆

Nanorods

Ag cocatalyst

ABSTRACT

Strontium niobates (SrNb₂O₆ and Sr₂Nb₂O₇) with regular nanostructures were synthesized by a facile flux method. Ag-loaded SrNb₂O₆ and Sr₂Nb₂O₇ exhibited different performances for the photocatalytic reduction of CO₂ in H₂O. Compared to Sr₂Nb₂O₇ nanoflakes and SrNb₂O₆ nanoparticles, SrNb₂O₆ nanorods exhibited higher photocatalytic activity and selectivity toward CO evolution. Stoichiometric amounts of CO (51.2 μmol h⁻¹) and H₂ (1.1 μmol h⁻¹) as the reduction products, in addition to O₂ (24.8 μmol h⁻¹) as the oxidation product, were obtained, indicating that H₂O serves as an electron donor in the photocatalytic conversion of CO₂. In addition, the effect of the Ag cocatalyst on the photocatalytic conversion of CO₂ was investigated.

© 2017 Elsevier B.V. All rights reserved.

1. Introduction

Carbon dioxide (CO₂), which is one of the major contributors to the greenhouse gas effect, has become a worldwide environmental burden because of fossil fuel consumption [1–4]. As a result, supplementing the natural carbon cycle and addressing climate change are imperative. The conversion of CO₂ to other valuable chemical compounds, e.g. CO, HCOOH, HCHO, CH₃OH, and CH₄, under ambient temperature and pressure conditions has attracted considerable attention as a sustainable strategy to solve environmental and energy issues [5–9], especially conversion of CO₂ into CO, which is widely studied in recent years as an alternative route to produce syngas components [10,11]. Since the discovery of the photoreduction of CO₂ into organic compounds using various semiconductors by Inoue et al. [5,12], several studies on the semiconductor-based photocatalytic conversion of CO₂ using H₂O as an electron donor have been reported [13–18]. Nevertheless, the selective activation of CO₂ by electrons and suppression of H₂ evolution in an aqueous solution are difficult because the redox potential of H⁺/H₂ (−0.41 V vs. NHE, at pH 7) is more positive than that of CO/CO₂ (−0.51 V

* Corresponding authors at: Department of Molecular Engineering, Graduate School of Engineering, Kyoto University, Kyoto 615-8510, Japan.

E-mail addresses: teramura@moleng.kyoto-u.ac.jp (K. Teramura), tanakat@moleng.kyoto-u.ac.jp (T. Tanaka).

vs. NHE, at pH 7) [19,20]. Previously, our group has reported high activity for Ag-loaded ZnGa₂O₄-modified Ga₂O₃ [21,22], La₂Ti₂O₇ [23], SrO-modified Ta₂O₅ [24], ZnGa₂O₄ [25], Sr₂KTa₅O₁₅ [26], and ZnTa₂O₆ [27] for the photocatalytic conversion of CO₂ by H₂O under UV irradiation. Ag cocatalysts are well known to be effective for the conversion of CO₂ to CO in aqueous solutions [12,28,29]. However, still only a few photocatalysts have been reported, which exhibit high activity and selectivity for the photocatalytic conversion of CO₂ by H₂O, even with the modification of a Ag cocatalyst. Hence, it is imperative to develop highly efficient photocatalysts for CO₂ reduction using water as the electron donor.

Niobium-containing materials, e.g., SrNb₂O₆ and Sr₂Nb₂O₇, have been reported as promising candidates for water splitting because of their attractive layered crystal structures, containing the [NbO₆] octahedra that can be distorted, and the high energy of the Nb 4d orbitals [30–34]. These structural advantages of niobium-based materials also make them promising for the photocatalytic reduction of CO₂. Nevertheless, only a few studies have reported the photocatalytic performance of niobium-based photocatalysts for CO₂ reduction, and the reported activities and selectivities were not satisfactory [35–37]. An erratic nanostructure for a photocatalyst has been reported to not only increase active sites for the photocatalytic reduction of CO₂ in the presence of H₂O but also promote the separation of oxidation and reduction sites because of its anisotropic effect [12,26,38,39].

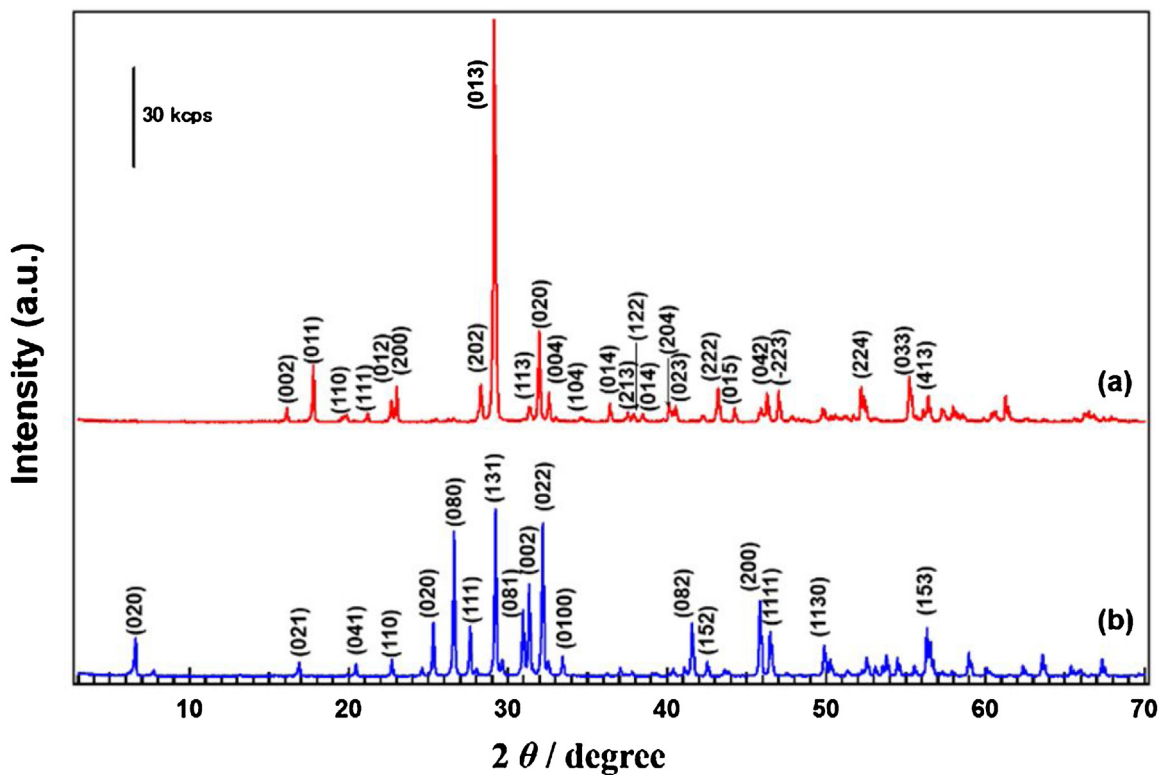


Fig. 1. XRD patterns of (a) SrNb_2O_6 and (b) $\text{Sr}_2\text{Nb}_2\text{O}_7$ fabricated by a flux method.

In this study, two strontium niobates (e.g. SrNb_2O_6 and $\text{Sr}_2\text{Nb}_2\text{O}_7$) with regular nanostructures were synthesized by a flux method, and their performance in the photocatalytic conversion of CO_2 in H_2O was investigated. After modification with a Ag cocatalyst, SrNb_2O_6 with a nanorod structure exhibited higher photocatalytic activity and selectivity toward CO evolution compared to $\text{Sr}_2\text{Nb}_2\text{O}_7$ with a nanoflake structure and SrNb_2O_6 with a nanoparticle structure. In addition, the effects of the Ag cocatalyst on the photocatalytic conversion of CO_2 were discussed.

2. Experimental

2.1. Photocatalyst preparation

SrNb_2O_6 and $\text{Sr}_2\text{Nb}_2\text{O}_7$ were prepared by a flux method. To fabricate SrNb_2O_6 , 2 g of Nb_2O_5 powder (99.9%, Wako) and 6 g of $\text{SrCl}_2 \cdot 6\text{H}_2\text{O}$ (99.9%, Wako) were ground in an alumina mortar for 5 min. $\text{SrCl}_2 \cdot 6\text{H}_2\text{O}$ was used as the precursor and flux reagent. The mixture was calcined in air using an alumina crucible at 1173 K for 2 h. After calcination, the obtained powder was thoroughly washed three times with hot water (353 K) to remove the residual salt and dried at 353 K in an oven. The process of synthesizing $\text{Sr}_2\text{Nb}_2\text{O}_7$ was almost the same as that of synthesizing SrNb_2O_6 , except for the use of SrCO_3 (99.9%, Wako) as the precursor. Modification using a Ag cocatalyst was performed by chemical reduction (CR), impregnation (IMP), and photodeposition (PD) methods. For modification by CR method, the obtained SrNb_2O_6 or $\text{Sr}_2\text{Nb}_2\text{O}_7$ (1.5 g) was suspended into a 50 mL aqueous solution of AgNO_3 (0.1 M), followed by the dropwise addition of a NaPH_2O_2 (0.4 M) solution into the suspension. After stirring the mixture at 358 K for 1.5 h, it was filtered and dried at room temperature. For modification by IMP method, SrNb_2O_6 (1.5 g) was homogeneously dispersed in an aqueous AgNO_3 solution, followed by evaporation at 358 K to remove water and calcination at 723 K for 2 h in air. Modification by PD method was carried out *in situ* during the photocatalytic

conversion of CO_2 . The synthetic details have been reported in our previous studies [24,27]. Generally, 1.5 g of SrNb_2O_6 powder was dispersed in 1.0 L of ultra-pure water containing a required amount of AgNO_3 , and the dissolved air in the solution was completely degassed by a flow of Ar gas. The suspension was irradiated under a 400 W high-pressure Hg lamp with a quartz filter using an inner-irradiation-type reaction vessel with Ar gas flowing for 1.5 h, followed by filtration and dried at room temperature.

2.2. Characterization

The crystal phase and structure of the samples were observed by powder X-ray diffractometry (Rigaku Multiflex) with $\text{Cu K}\alpha$ radiation ($\lambda = 0.154 \text{ nm}$) at a scan rate of 4° min^{-1} . Sample morphologies were observed by field-emission scanning electron microscopy (FE-SEM, SU-8220, Hitachi High Technologies) and transmission electron microscopy (TEM, JEM-2100F). The Brunauer–Emmett–Teller surface areas of the photocatalysts were measured by their N_2 adsorption isotherms at 77 K using a volumetric gas adsorption apparatus (BELSORP-mini II, BEL Japan, Inc.). Prior to the measurements, each sample was evacuated at 473 K for 1 h using a pretreatment system (BELPREP-vacII, BEL Japan, Inc.). UV-vis diffuse-reflectance spectra were recorded on a UV-visible spectrometer (V-650, JASCO) equipped with an integrated sphere accessory.

2.3. Photocatalytic reaction

The photocatalytic conversion of CO_2 was carried out using a flow system with an inner-irradiation-type reaction vessel at ambient pressure. First, the synthesized photocatalyst (0.5 g) was dispersed in ultrapure water (1.0 L) containing 0.1 M NaHCO_3 . Second, CO_2 was bubbled into the solution at a flow rate of 30 mL min^{-1} . Third, the suspension was illuminated using a 400-W high-pressure mercury lamp with a quartz filter connected to a

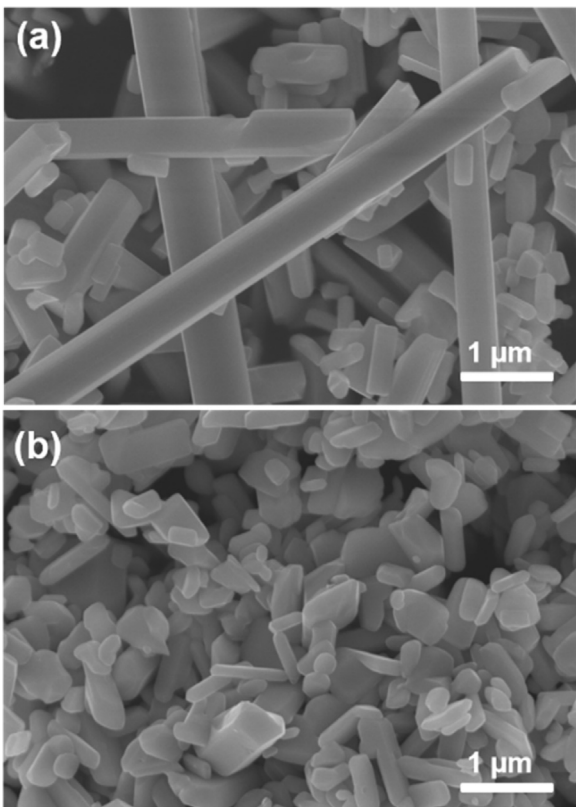


Fig. 2. SEM images of as-prepared (a) SrNb_2O_6 and (b) $\text{Sr}_2\text{Nb}_2\text{O}_7$ prepared by the flux method.

water cooling system. The amounts of the evolved H_2 and O_2 were detected using a thermal conductivity detector–gas chromatography system (TCD–GC, Shimadzu Corp; MS-5A column, Ar carrier). The amount of evolved CO was analyzed by a flame ionization detector–GC with a methanizer (ShinCarbon ST column, N_2 carrier). The selectivity toward CO evolution compared to H_2 evolution and the balance between the consumed electrons (e^-) and holes (h^+) were expressed by Eqs. (1) and (2), respectively:

$$\text{Selectivity toward CO evolution}(\%) = 100 \times 2R_{\text{CO}} / (2R_{\text{CO}} + 2R_{\text{H}_2}) \quad (1)$$

$$\text{Consumed } e^- / h^+ = (2R_{\text{CO}} + 2R_{\text{H}_2}) / 4R_{\text{O}_2}. \quad (2)$$

Here, R_{CO} and R_{H_2} represent the formation rates of CO and H_2 , respectively.

In the isotopic experiment, $^{12}\text{CO}_2$ was replaced by $^{13}\text{CO}_2$. The formation rates of H_2 , O_2 , ^{13}CO , and ^{12}CO under photoirradiation were detected using a quadrupole mass spectrometer (BELMASS, Microtrac BEL) combined with a TCD–GC detector, the reactor set-up is shown in Fig. S1.

3. Results and discussion

Fig. 1 shows the XRD patterns of as-prepared SrNb_2O_6 and $\text{Sr}_2\text{Nb}_2\text{O}_7$ fabricated by a flux method. All the diffraction peaks in the upper and lower patterns were accurately indexed to the pure monoclinic phase of SrNb_2O_6 with a $\text{P}12_1/c$ space group (JCPDS 72-2088) and the orthorhombic phase of $\text{Sr}_2\text{Nb}_2\text{O}_7$ with a $\text{Cmc}2_1$ space group (JCPDS 70-0114), respectively [32]. No peaks corresponding to other impurity phases were observed, indicating that the pure phases of SrNb_2O_6 and $\text{Sr}_2\text{Nb}_2\text{O}_7$ are successfully prepared by calcination at 1173 K for 2 h by the flux method. Fig.

S2A shows the UV–vis diffuse reflectance spectra of as-synthesized SrNb_2O_6 and $\text{Sr}_2\text{Nb}_2\text{O}_7$; diffuse reflectance spectra were converted to absorption spectra using the Kubelka–Munk equation. The band gaps of $\text{Sr}_2\text{Nb}_2\text{O}_7$ and SrNb_2O_6 were estimated as 3.97 eV and 3.86 eV, respectively (Fig. S2B), based on the Davis–Mott equation [40] using the Kubelka–Munk function $F(R_\infty)$ obtained from the diffuse-reflectance spectrum; these values are similar to the reported values [31,32].

$$[F(R_\infty)\text{hv}] = A(h\nu - E_g)^n. \quad (3)$$

Here, h , ν , A , and $n = 1/2$ represent the Planck's constant, vibrational frequency, proportionality constant, and direct allowed transition, respectively.

Fig. 2 shows the SEM images of as-prepared SrNb_2O_6 and $\text{Sr}_2\text{Nb}_2\text{O}_7$. SrNb_2O_6 predominantly consisted of 1D rod-like particles (Fig. 2a). The diameters of the nanorods ranged from 100 nm to 1 μm , and their lengths ranged from 500 nm to several tens of microns. On the other hand, $\text{Sr}_2\text{Nb}_2\text{O}_7$ prepared by the same flux method predominantly exhibited a nanoflake structure with a thickness of 50–250 nm (Fig. 2b). The surface areas of SrNb_2O_6 nanorod and $\text{Sr}_2\text{Nb}_2\text{O}_7$ nanoflake were $1.78 \text{ m}^2 \text{ g}^{-1}$ and $3.85 \text{ m}^2 \text{ g}^{-1}$, respectively.

Fig. 3 shows the formation rates of H_2 , O_2 , and CO for the photocatalytic conversion of CO_2 by H_2O over $\text{Ag}/\text{SrNb}_2\text{O}_6$ and $\text{Ag}/\text{Sr}_2\text{Nb}_2\text{O}_7$ under UV light irradiation. Ag (1.0 wt%) was loaded as the cocatalyst on the sample surface by chemical reduction method. The surface areas of $\text{Ag}/\text{SrNb}_2\text{O}_6$ and $\text{Ag}/\text{Sr}_2\text{Nb}_2\text{O}_7$ were $2.25 \text{ m}^2 \text{ g}^{-1}$ and $4.26 \text{ m}^2 \text{ g}^{-1}$, respectively; these values are slightly greater than that of the bare catalyst. High selectivity (greater than 95%) toward the photocatalytic evolution of CO over $\text{Ag}/\text{SrNb}_2\text{O}_6$ was observed. CO was obtained as the main product ($44.1 \mu\text{mol h}^{-1}$), with marginal amounts of H_2 ($2.7 \mu\text{mol h}^{-1}$). A stoichiometric formation amount of O_2 ($22.4 \mu\text{mol h}^{-1}$), in addition to H_2 and CO , was observed, indicating that H_2O serves as the electron donor for the photocatalytic reduction of CO_2 . On the other hand, compared to $\text{Ag}/\text{SrNb}_2\text{O}_6$, $\text{Ag}/\text{Sr}_2\text{Nb}_2\text{O}_7$ exhibited lower formation rates of H_2 , CO , and O_2 ; H_2 was the main product; and the photocatalytic activity also rapidly decreased after photoirradiation for 5 h. This result clearly indicated that $\text{Ag}/\text{SrNb}_2\text{O}_6$ with a nanorod structure exhibits better photocatalytic activity and higher selectivity toward CO evolution compared to $\text{Ag}/\text{Sr}_2\text{Nb}_2\text{O}_7$ with a nanoflake structure.

As SrNb_2O_6 and $\text{Sr}_2\text{Nb}_2\text{O}_7$ exhibited different structures, SrNb_2O_6 with a nanorod structure was compared with catalysts with other nanostructures synthesized by the solid-state reaction (SSR) and solvothermal methods. As shown in the XRD patterns (Fig. S3), a pure SrNb_2O_6 phase was successfully prepared, except using the SSR method, which contained few impurity phases of $\text{Sr}_2\text{Nb}_2\text{O}_7$. From the SEM images shown in Fig. 4, aggregated nanoparticles (Fig. 4a) and a mixture of nanoparticles and nanorods (Fig. 4b) were observed for SrNb_2O_6 fabricated by SSR and the solvothermal method, respectively. All of the Ag -loaded SrNb_2O_6 products were favorable for CO evolution; however, SrNb_2O_6 nanorods prepared by the flux method exhibited higher photocatalytic activity and selectivity toward CO evolution compared to the aggregated nanoparticles prepared by SSR and the solvothermal method (Fig. 4c). On the other hand, the nanorod-containing SrNb_2O_6 products prepared by the solvothermal method also exhibited higher photocatalytic selectivity toward CO evolution although its photocatalytic activity was less than that of the SrNb_2O_6 nanoparticles synthesized by the SSR method. This result revealed that $\text{Ag}/\text{SrNb}_2\text{O}_6$ is promising for the photocatalytic conversion of CO_2 , and the nanorod structure is favorable for CO evolution, the reasons for the high selectivity toward CO evolution of SrNb_2O_6 nanorod will be discussed later.

Fig. 5 shows the blank tests using the SrNb_2O_6 nanorods. No product was detected in the dark (Fig. 5a) and without a photocat-

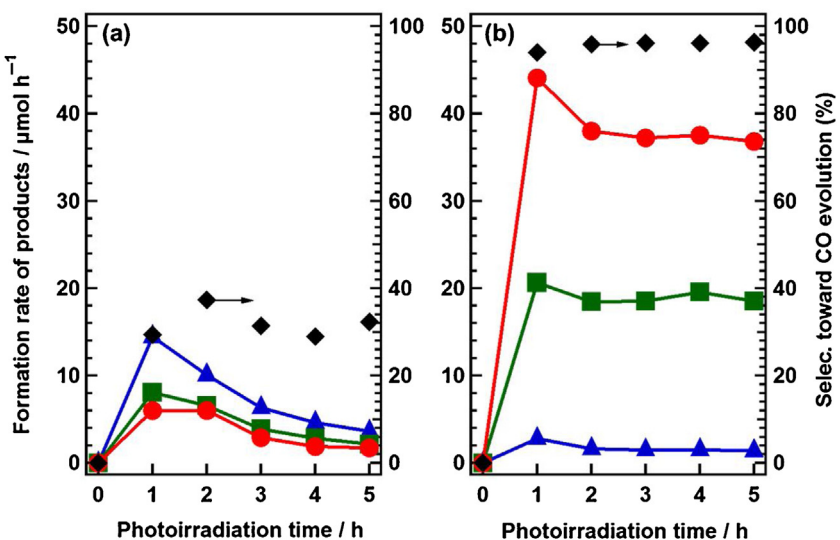


Fig. 3. Formation rates of H_2 (blue triangle), O_2 (green square), and CO (red circle) and the selectivity toward CO evolution (black diamond) for the photocatalytic conversion of CO_2 in an aqueous NaHCO_3 solution using (a) $\text{Ag/SrNb}_2\text{O}_6$ and (b) $\text{Ag/Sr}_2\text{Nb}_2\text{O}_7$ as the photocatalysts. Photocatalyst powder: 0.5 g, reaction solution volume: 1.0 L, additive: 0.1 M NaHCO_3 , Ag loading amount: 1.0 wt%, modification method: chemical reduction, CO_2 flow rate: 30 mL min^{-1} , light source: 400-W high-pressure Hg lamp. (For interpretation of the references to color in this figure legend, the reader is referred to the web version of this article.)

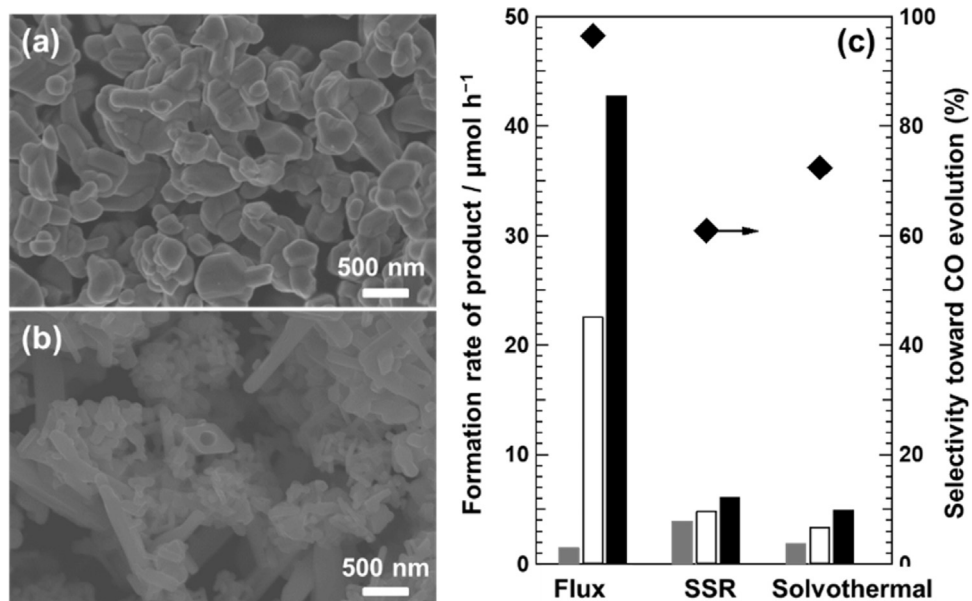


Fig. 4. SEM images of the SrNb_2O_6 products prepared using different methods: (a) SSR method, (b) Solvothermal method; (c) Formation rates of H_2 (blue), O_2 (green), and CO (black) and the selectivity toward CO evolution (black diamond) for the photocatalytic conversion of CO_2 in an aqueous. Photocatalyst powder: 0.5 g, reaction solution volume: 1.0 L, additive: 0.1 M NaHCO_3 , Ag loading amount: 1.0 wt%, modification method: chemical reduction, CO_2 flow rate: 30 mL min^{-1} , light source: 400-W high-pressure Hg lamp. (For interpretation of the references to color in this figure legend, the reader is referred to the web version of this article.)

Table 1
Effects of reactant solutions on the photocatalytic reduction of CO_2 over $\text{Ag/SrNb}_2\text{O}_6$.^a

Additive (mol L^{-1})	pH ^b	Formation rate of products/ $\mu\text{mol h}^{-1}$			Selec. toward CO (%)
		H_2	O_2	CO	
None	4.1	8.1	4.2	0.3	3.6
NaHCO_3 (0.1)	6.8	2.8	20.1	44.1	94.0
Na_2CO_3 (0.05)	7.0	2.2	23.0	49.7	95.8
NaOH (0.1)	6.9	3.8	24.4	45.2	92.3
NaCl (0.1)	3.	10.7	5.8	1.2	9.8
H_2SO_4 (0.05)	1.3	176.5	85.0	0.1	0.1

^a Photocatalyst powder: 0.5 g, reaction solution volume: 1.0 L, additive: 0.1 M NaHCO_3 , Ag loading amount: 1.0 wt%, modification method: chemical reduction, CO_2 flow rate: 30 mL min^{-1} , light Source: 400-W high-pressure Hg lamp.

^b During the photocatalytic reduction of CO_2 .

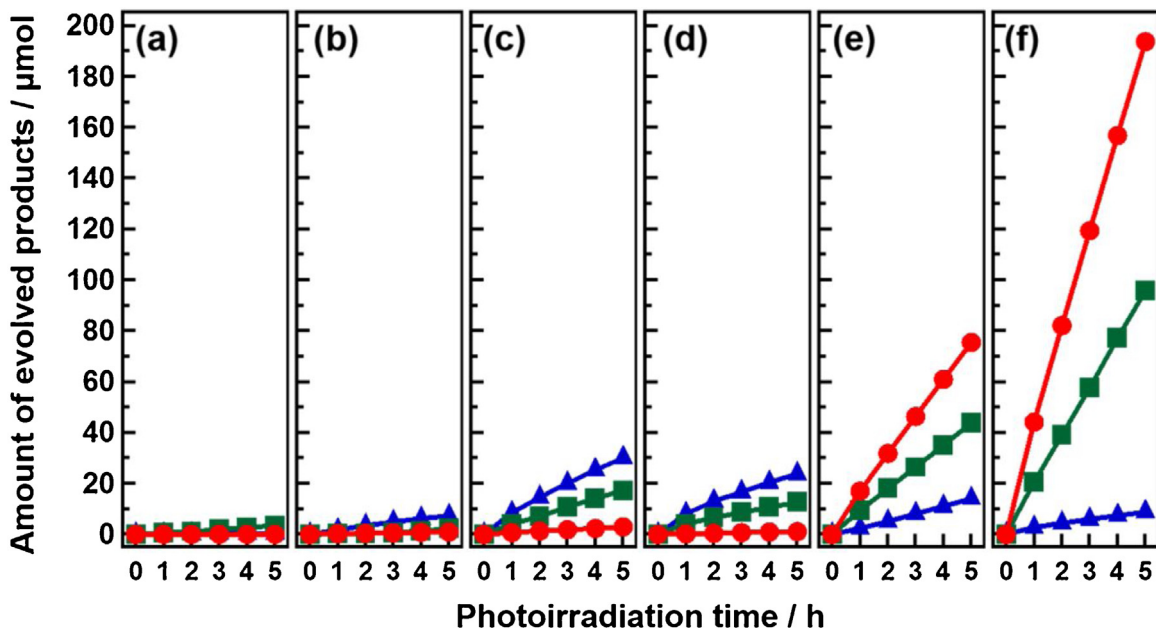


Fig. 5. Amounts of H_2 (blue triangle), O_2 (green square), and CO (red circle) from control experiments for the photocatalytic conversion of CO_2 in water using the $\text{Ag/SrNb}_2\text{O}_6$ photocatalyst. (a) dark condition; (b) no photocatalyst; (c) no additive; (d) no Ag cocatalyst; (e) with Ar gas flow; (f) typical condition. Photocatalyst powder: 0.5 g, reaction solution volume: 1.0 L, additive: 0.1 M NaHCO_3 , Ag loading amount: 1.0 wt%, modification method: chemical reduction, CO_2 flow rate: 30 mL min^{-1} , light source: 400-W high-pressure Hg lamp. (For interpretation of the references to color in this figure legend, the reader is referred to the web version of this article.)

alyst (Fig. 5b). Marginal amounts of H_2 and O_2 were observed, while the formation rates of CO were rather low without a NaHCO_3 additive and a Ag cocatalyst (Fig. 5c and d), indicating that the NaHCO_3 additive and Ag cocatalyst are indispensable for the photocatalytic conversion of CO_2 in an aqueous solution. The use of inert Ar instead of CO_2 led to the decreased formation rate of evolved CO (Fig. 5e). The best performance for the photocatalytic conversion of CO_2 was using Ag-loaded SrNb_2O_6 nanorods in an aqueous NaHCO_3 solution with bubbling CO_2 under photoirradiation (Fig. 5f). From the photocatalytic result mentioned above, the SrNb_2O_6 nanorods clearly exhibited good activity for the photocatalytic conversion of CO_2 by H_2O under UV irradiation. The stoichiometric formation amount of H_2 , CO , and O_2 indicated that H_2O serves as electron donor for the photocatalytic reduction of CO_2 .

It is known that gaseous CO_2 can dissolve in an aqueous solution, whereas, it is negligible in pure water [41]. Adding additives in the aqueous solution could greatly affect the solubility of gaseous CO_2 and pH value into a reactant solution for CO_2 reduction [42]. The effects of bases on the photocatalytic conversion of CO_2 over $\text{Ag/SrNb}_2\text{O}_6$ are shown in Table 1. When NaHCO_3 (0.1 mol L^{-1}), Na_2CO_3 (0.05 mol L^{-1}), and NaOH (0.1 mol L^{-1}) were added into the reactant solution, it showed similar formation rates of products and pH values for the photocatalytic conversion of CO_2 . Because CO_2 gas was continuously bubbled in solution, all the concentrations of CO_2 (aq), HCO_3^- , and CO_3^{2-} achieve equilibrium in case that Na_2CO_3 and NaOH are added as well as NaHCO_3 [42]. In our previous work, the concentration of CO_2 (aq), HCO_3^- , and CO_3^{2-} in 0.1 mol L^{-1} NaHCO_3 aqueous solution were calculated under different pH values, which showed higher dissolved amount of CO_2 (aq) for the photocatalytic conversion of CO_2 (at pH = 6.8) as compared to that in the pure water [43]. Whereas, in the solutions of 0.05 mol L^{-1} H_2SO_4 and 0.1 mol L^{-1} NaCl , the SO_4^{2-} and Cl^- ions are hard to keep the high solubility of gaseous CO_2 in solution, the concentrations of CO_2 related species are similar to that in H_2O during the bubbling of CO_2 [42]. On the other hand, the high concentration of H^+ in H_2SO_4 and NaCl solutions is in favor of water splitting, so H_2 was the main products when H_2SO_4 and NaCl were used as additives.

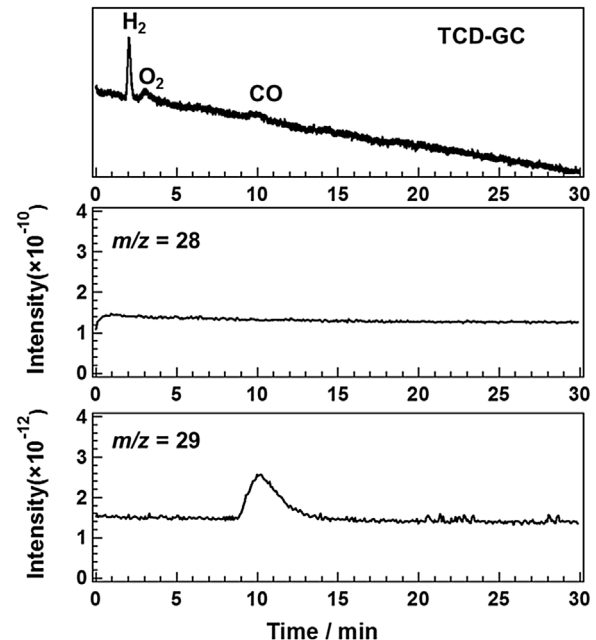


Fig. 6. Gas chromatograms and mass spectra (m/z 28, 29) for the photocatalytic conversion of $^{13}\text{CO}_2$ by H_2O over $\text{Ag/SrNb}_2\text{O}_6$. Photocatalyst powder: 0.5 g, reaction solution volume: 1.0 L, Ag loading amount: 1.0 wt%, modification method: chemical reduction, $^{13}\text{CO}_2$ gas flow rate: 30 mL min^{-1} , light source: 400-W high-pressure Hg lamp.

Fig. 6 shows the gas chromatograms and mass spectra for the photocatalytic conversion of $^{13}\text{CO}_2$ by H_2O over $\text{Ag/SrNb}_2\text{O}_6$. Peaks corresponding to H_2 , O_2 , and CO were observed in the TCD-GC chromatogram. The peak at m/z 29 corresponded to ^{13}CO ; in contrast, no peak was detected at m/z 28. Therefore, CO evolved over $\text{Ag/SrNb}_2\text{O}_6$ originates from the CO_2 introduced in the gas phase and not from the residual organic contaminants on the surface.

Loading with Ag has been reported to affect the activity and selectivity for the photocatalytic reduction of CO_2 [25]. Fig. 7 shows

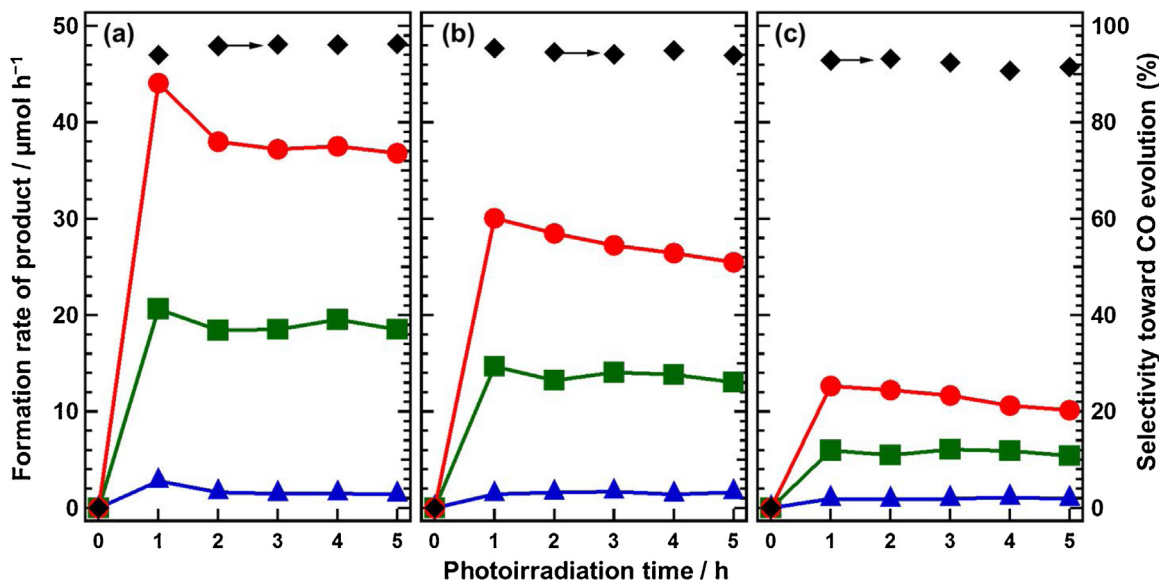


Fig. 7. Formation rates of H₂ (blue triangle), O₂ (green square), and CO (red circle) and the selectivity toward CO evolution (black diamond) for the photocatalytic conversion of CO₂ in an aqueous NaHCO₃ solution using Ag-modified SrNb₂O₆ by (a) CR, (b) IMP, and (c) PD methods. Photocatalyst powder: 0.5 g, reaction solution volume: 1.0 L, additive: 0.1 M NaHCO₃, Ag loading amount: 1.0 wt%, CO₂ flow rate: 30 mL min⁻¹, light source: 400-W high-pressure Hg lamp. (For interpretation of the references to color in this figure legend, the reader is referred to the web version of this article.)

the formation rates of H₂, O₂, and CO for the photocatalytic conversion of CO₂ in an aqueous NaHCO₃ solution using Ag/SrNb₂O₆ modified by CR, IMP, and PD method. Ag-loaded SrNb₂O₆ prepared by all methods exhibited high photocatalytic selectivity toward CO evolution, and stoichiometric formation amount of H₂, CO, and O₂ were obtained. The amount of CO obtained as the reduction product of CO₂ over Ag/SrNb₂O₆ prepared by CR method was greater than those obtained by IMP and PD methods. The photocatalytic activity clearly decreased after photoirradiation for 1 h and gradually became stable with the increase in the photoirradiation time using CR methods. However, the evolution rate of CO only slightly decreased during photoirradiation for 5 h by the loading of Ag using PD method.

Fig. 8 shows the SEM images of Ag/SrNb₂O₆ prepared by the three methods. Ag particles modified by CR method were uniformly scattered on the SrNb₂O₆ nanorod surface with a size less than 10 nm (Fig. 8a). Ag cocatalysts prepared by IMP method were dispersed on the surface of SrNb₂O₆ nanorod with an aggregate size of 10–50 nm (Fig. 8b). The Ag cocatalysts prepared by PD method were predominantly deposited on the top of SrNb₂O₆ nanorods as nanoparticles with a size of 30–70 nm (Fig. 8c). This selective deposition of Ag cocatalysts was also observed for Ag/SrNb₂O₆ prepared by CR and IMP methods at a photoirradiation time of 1 h (Fig. 8d and e). The sizes of the Ag particles, which were prepared by CR and IMP methods, redeposited on the top of nanorods were 10–30 nm and 20–70 nm, respectively. The particle size of Ag on the top of nanorods was almost similar to the initial size of Ag/SrNb₂O₆ prepared by PD method after photoirradiation for 5 h (Fig. 8f). Ag particles loaded on the top plane with a smaller size prepared by CR method exhibited higher photocatalytic activity for the reduction of CO₂ than those prepared by IMP and PD method. This result is consistent with those reported previously [12].

Fig. 9 shows the effect of the Ag cocatalyst loading amount on the photocatalytic activity for CO₂ conversion. Modification of the catalyst with marginal amounts of Ag dramatically improved the formation rate of CO and suppressed the formation rate of H₂, indicating that the modification of the Ag cocatalyst leads to increased reaction sites on the SrNb₂O₆ nanorod surface for the reduction of CO₂ because of its good selectivity toward CO evolution [28]. As the active sites for reduction increased with increasing amounts

of added Ag cocatalyst, the formation rate of CO increased with the addition of a large amount of Ag from 0 to 0.5 wt%. However, further increase in the amount of Ag led to the aggregation of Ag particles; hence, the photocatalytic activity decreases with the further modification by Ag with a loading from 0.5 to 2 wt%. The particle size of the Ag cocatalysts increased with the increase in the Ag loading amount, followed by gradual aggregation, which was clearly observed from the SEM and TEM images in Fig. S4. The highest formation rate of the evolved CO (51.2 μmol h⁻¹) was observed using 0.5 wt% Ag-loaded SrNb₂O₆ nanorods, as well as high selectivity (98%), although the conversion efficiency was very low (0.06%).

Fig. 10 shows the time course for the evolution of CO, H₂, and O₂ during the photocatalytic conversion of CO₂ by H₂O over 0.5 wt% Ag-loaded SrNb₂O₆. Stable selectivity toward CO was observed during photoirradiation (approximately 97%). CO was evolved as the main reduction product, and marginal amounts of H₂ were generated. Stoichiometric amounts of O₂ as the oxidation product of H₂O were obtained, in addition to CO and H₂ as the reduction products, suggesting that H₂O serves as the electron donor for the photocatalytic conversion of CO₂. Notably, the formation rate of CO gradually decreased with the increase in the photoirradiation time for the first 6 h and then was maintained constant. As shown in the XRD pattern (Fig. S5), the crystalline structures of SrNb₂O₆ were very stable under UV light irradiation, while the diffraction peak corresponding to metallic Ag was not observed because of the low amount of Ag.

Fig. 11 shows the TEM images, which clearly show the variation of Ag particles on the SrNb₂O₆ nanorod surface. Before the loading of Ag, a smooth SrNb₂O₆ nanorod surface was observed (Fig. 11a). After the loading of the Ag cocatalyst by CR method, Ag nanoparticles with a size less than 10 nm were highly dispersed on the SrNb₂O₆ nanorod surface (Fig. 11b), which were selectively redeposited on the top of the SrNb₂O₆ nanorod with photoirradiation (Fig. 11c). The particle size of Ag increased with the increase in the photoirradiation time from 0 h to 6 h (Fig. 11d) and gradually maintained constant with the further increase in the photoirradiation time to 15 h (Fig. 11e and f). The variation of Ag particles could also be confirmed by EDS analysis (Fig. S6).

Pt and PbO₂ have been reported to be reductively and oxidatively photodeposited, respectively, on surfaces because of their

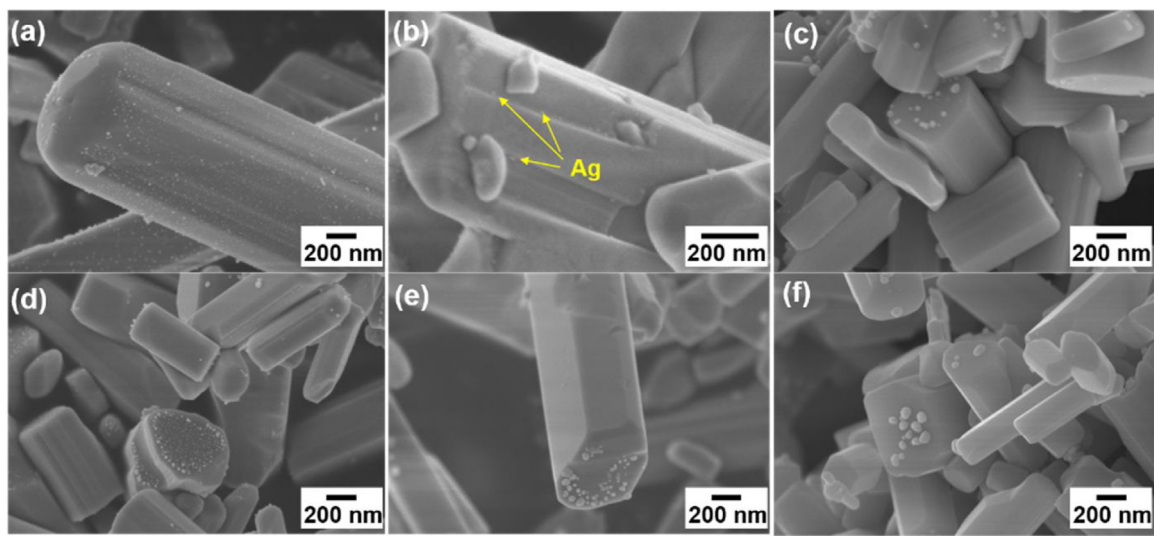


Fig. 8. SEM images of SrNb_2O_6 modified with Ag by (a), (d) CR, (b), (e) IMP, and (c), (f) PD methods. (a–c) before and (d–f) after photoirradiation for 1 h. Ag loading amount: 1.0 wt%.

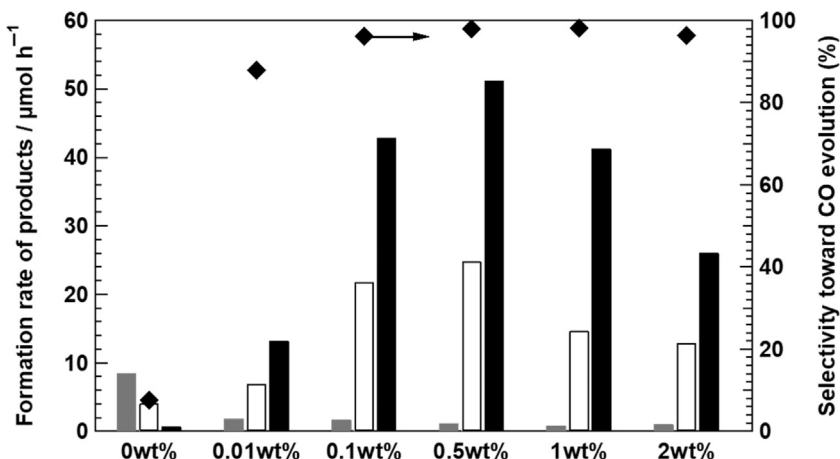


Fig. 9. Formation rates of H_2 (blue), O_2 (green), and CO (red) and selectivity toward CO (black diamond) evolution for the photocatalytic conversion of CO_2 in an aqueous NaHCO_3 solution using the SrNb_2O_6 photocatalyst modified with different contents of Ag. Photocatalyst powder: 0.5 g, reaction solution volume: 1.0 L, additive: 0.1 M NaHCO_3 , modification method: chemical reduction, CO_2 flow rate: 30 mL min^{-1} , light source: 400-W high-pressure Hg lamp. (For interpretation of the references to color in this figure legend, the reader is referred to the web version of this article.)

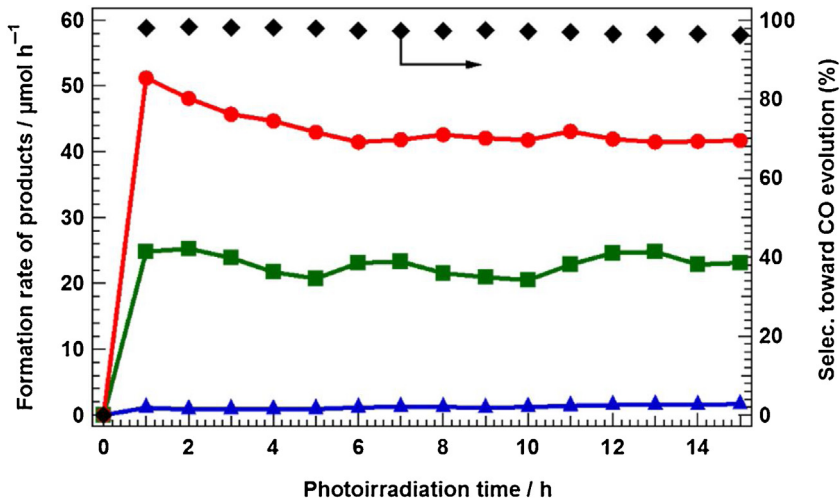


Fig. 10. Time course for the evolution of CO (red circle), O_2 (green square), and H_2 (blue triangle) evolution and the selectivity toward CO evolution (black diamond) for the photocatalytic conversion of CO_2 in an aqueous NaHCO_3 solution using $\text{Ag/SrNb}_2\text{O}_6$. Photocatalyst powder: 0.5 g, reaction solution volume: 1.0 L, additive: 0.1 M NaHCO_3 , Ag loading amount: 0.5 wt%, modification method: chemical reduction, CO_2 flow rate: 30 mL min^{-1} , light source: 400-W high-pressure Hg lamp. (For interpretation of the references to color in this figure legend, the reader is referred to the web version of this article.)

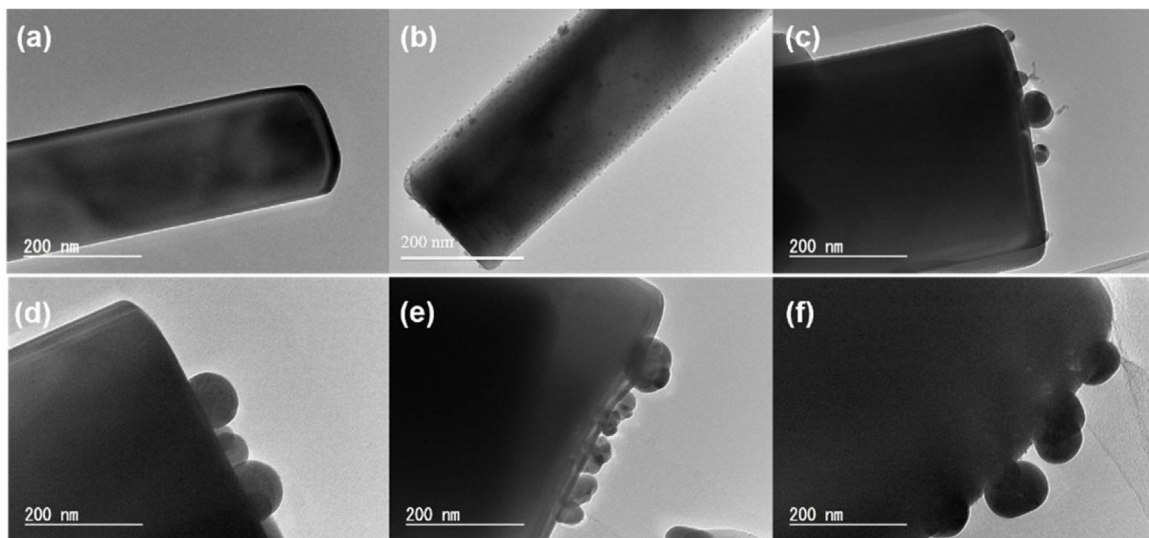
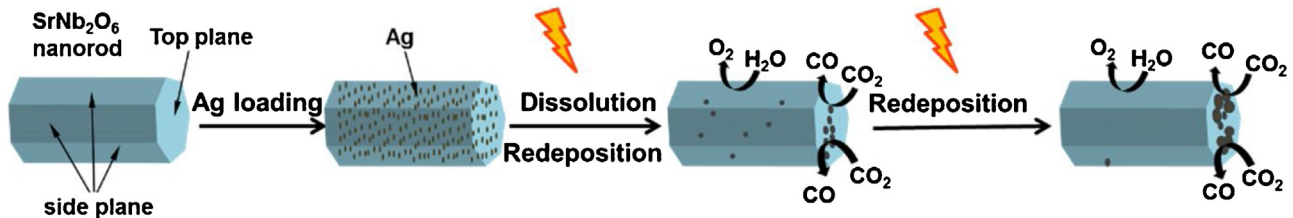


Fig. 11. TEM images of (a) SrNb_2O_6 and Ag-loaded SrNb_2O_6 nanorods at different photoirradiation times: (b) 0 h, (c) 3 h, (d) 6 h, (e) 10 h, (f) 15 h. Ag loading amount: 0.5 wt%, modification method: chemical reduction.



Scheme 1. Possible mechanism for the redeposition of the Ag cocatalyst on the Ag/ SrNb_2O_6 nanorod surface.

anisotropic properties [38,44]. Hence, a series of metals and PbO_2 is examined to investigate the anisotropy property of the SrNb_2O_6 nanorod (Fig. S7). Metallic Au, Pt, and Pd were reductively photodeposited from $[\text{AuCl}_4]^-$, $[\text{PtCl}_6]^{2-}$, and Pd^{2+} on the top plane of the nanorod, respectively. In contrast, PbO_2 was selectively deposited from Pb^{2+} on the side plane of the nanorod, which was also confirmed by EDS (Fig. S8). This selective photodeposition of different materials demonstrated that reduction and oxidation by the photo-generated e^- and h^+ primarily occur on the top and side planes of the nanorods, respectively, indicating that Ag loaded on the SrNb_2O_6 surface in this study is firstly dissolved by the photogenerated holes to Ag^+ and then redeposited on the top plane under photoirradiation because of the anisotropy of the SrNb_2O_6 nanorod.

Scheme 1 shows the possible mechanism for the redeposition of the Ag cocatalyst on the Ag/ SrNb_2O_6 nanorod surface. The photocatalytic reduction of CO_2 predominantly led to the formation of CO on the top of the Ag-loaded SrNb_2O_6 nanorods, while O_2 was formed on the sides of the nanorods. The variation of the Ag particles on the SrNb_2O_6 nanorod surface, which were dissolved and redeposited on the top of SrNb_2O_6 nanorod possibly led to the decreased Ag active sites; hence, the photocatalytic activity decreases during photoirradiation, especially in the first 1 h. The separation of the reduction sites from the oxidation sites contributed to the decrease in the recombination of the photogenerated carriers; hence, Ag-loaded SrNb_2O_6 nanorods prepared by the flux method exhibit good activity and selectivity for the photocatalytic conversion of CO_2 .

4. Conclusion

SrNb_2O_6 nanorods and $\text{Sr}_2\text{Nb}_2\text{O}_7$ nanoflakes were successfully synthesized by a flux method. SrNb_2O_6 with a nanorod structure exhibited higher photocatalytic activity and selectivity toward CO evolution for the photocatalytic conversion of CO_2 compared to $\text{Sr}_2\text{Nb}_2\text{O}_7$ nanoflakes and SrNb_2O_6 particles. Ag particles loaded on the SrNb_2O_6 nanorod surface with a smaller size exhibited higher photocatalytic activity for CO_2 conversion. The Ag cocatalysts loaded by CR method were uniformly loaded on the SrNb_2O_6 nanorod surface, followed by the selective re-deposition on the top of SrNb_2O_6 nanorod during photoirradiation. The separation of the reduction and oxidation sites was considered to be crucial for the high photocatalytic activity and selectivity toward CO evolution for CO_2 conversion.

Acknowledgments

This study was partially supported by a Grant-in-Aid for Scientific Research on Innovative Areas “All Nippon Artificial Photosynthesis Project for Living Earth” [grant number 2406] of the Ministry of Education, Culture, Sports, Science, and Technology (MEXT) of Japan, the Precursory Research for Embryonic Science and Technology, supported by the Japan Science and Technology Agency, and the Program for Elements Strategy Initiative for Catalysts & Batteries, commissioned by the MEXT of Japan. Rui PANG thanks the State Scholarship of China Scholarship Council, affiliated with the Ministry of Education of the P.R. China.

Appendix A. Supplementary data

Supplementary data associated with this article can be found, in the online version, at <http://dx.doi.org/10.1016/j.apcatb.2017.06.052>.

References

- [1] J. Hansen, L. Nazarenko, R. Ruedy, M. Sato, J. Willis, A. Del Genio, D. Koch, A. Lacis, K. Lo, S. Menon, Earth's energy imbalance: confirmation and implications, *Science* 308 (2005) 1431–1435.
- [2] W. Wang, S. Wang, X. Ma, J. Gong, Recent advances in catalytic hydrogenation of carbon dioxide, *Chem. Soc. Rev.* 40 (2011) 3703–3727.
- [3] M. Mikkelsen, M. Jørgensen, F.C. Krebs, The teraton challenge. A review of fixation and transformation of carbon dioxide, *Energy Environ. Sci.* 3 (2010) 43–81.
- [4] A.J. Morris, G.J. Meyer, E. Fujita, Molecular approaches to the photocatalytic reduction of carbon dioxide for solar fuels, *Acc. Chem. Res.* 42 (2009) 1983–1994.
- [5] T. Inoue, A. Fujishima, S. Konishi, K. Honda, Photoelectrocatalytic reduction of carbon dioxide in aqueous suspensions of semiconductor powders, *Nature* 277 (1979) 637–638.
- [6] B. Kumar, M. Llorente, J. Froehlich, T. Dang, A. Sathrum, C.P. Kubiak, Photochemical and photoelectrochemical reduction of CO_2 , *Annu. Rev. Phys. Chem.* 63 (2012) 541–569.
- [7] R.K. Yadav, G.H. Oh, N.-J. Park, A. Kumar, K.-J. Kong, J.-O. Baeg, Highly selective solar-driven methanol from CO_2 by a photocatalyst/biocatalyst integrated system, *J. Am. Chem. Soc.* 136 (2014) 16728–16731.
- [8] G. Qin, Y. Zhang, X. Ke, X. Tong, Z. Sun, M. Liang, S. Xue, Photocatalytic reduction of carbon dioxide to formic acid, formaldehyde, and methanol using dye-sensitized TiO_2 film, *Appl. Catal. B: Environ.* 129 (2013) 599–605.
- [9] E.V. Kondratenko, G. Mul, J. Baltrusaitis, G.O. Larrazábal, J. Pérez-Ramírez, Status and perspectives of CO_2 conversion into fuels and chemicals by catalytic, photocatalytic and electrocatalytic processes, *Energy Environ. Sci.* 6 (2013) 3112–3135.
- [10] M. Asadi, B. Kumar, A. Behranginia, B.A. Rosen, A. Baskin, N. Repnin, D. Pisasale, P. Phillips, W. Zhu, R. Haasch, Robust carbon dioxide reduction on molybdenum disulphide edges, *Nat. Commun.* 5 (2014) 4470, <http://dx.doi.org/10.1038/ncomms5470>.
- [11] Q. Lu, J. Rosen, Y. Zhou, G.S. Hutchings, Y.C. Kimmel, J.G. Chen, F. Jiao, A selective and efficient electrocatalyst for carbon dioxide reduction, *Nat. Commun.* 5 (2014) 3242, <http://dx.doi.org/10.1038/ncomms4242>.
- [12] H. Inoue, T. Matsuyama, B.J. Liu, T. Sakata, H. Mori, H. Yoneyama, Photocatalytic activities of TiO_2 , microcrystals prepared in SiO_2 matrixes using a sol-gel method for carbon dioxide reduction, *Chem. Lett.* (1994) 653–656.
- [13] N.M. Dimitrijevic, B.K. Vijayan, O.G. Poluektov, T. Rajh, K.A. Gray, H. He, P. Zapol, Role of water and carbonates in photocatalytic transformation of CO_2 to CH_4 on titania, *J. Am. Chem. Soc.* 133 (2011) 3964–3971.
- [14] K. Iizuka, T. Wato, Y. Miseki, K. Saito, A. Kudo, Photocatalytic reduction of carbon dioxide over Ag cocatalyst-loaded $\text{Al}_{4-x}\text{Ti}_4\text{O}_{15}$ ($\text{A}=\text{Ca, Sr, and Ba}$) using water as a reducing reagent, *J. Am. Chem. Soc.* 133 (2011) 20863–20868.
- [15] C. Wang, R.L. Thompson, J. Baltrus, C. Matranga, Visible light photoreduction of CO_2 using $\text{CdSe}/\text{Pt}/\text{TiO}_2$ heterostructured catalysts, *J. Phys. Chem. Lett.* 1 (2009) 48–53.
- [16] Q. Kang, T. Wang, P. Li, L. Liu, K. Chang, M. Li, J. Ye, Photocatalytic reduction of carbon dioxide by hydrous hydrazine over Au–Cu alloy nanoparticles supported on $\text{SrTiO}_3/\text{TiO}_2$ coaxial nanotube arrays, *Angew. Chem. Int. Ed.* 54 (2015) 841–845.
- [17] L. Zhang, W. Wang, D. Jiang, E. Gao, S. Sun, Photoreduction of CO_2 on BiOCl nanoplates with the assistance of photoinduced oxygen vacancies, *Nano Res.* 8 (2015) 821–831.
- [18] J.-C. Wang, H.-C. Yao, Z.-Y. Fan, L. Zhang, J.-S. Wang, S.-Q. Zang, Z.-J. Li, Indirect Z-scheme $\text{BiO}/\text{g-C}_3\text{N}_4$ photocatalysts with enhanced photoreduction CO_2 activity under visible light irradiation, *ACS Appl. Mater. Interfaces* 8 (2016) 3765–3775.
- [19] J.L. White, M.F. Baruch, J.E. Pander III, Y. Hu, I.C. Fortmeyer, J.E. Park, T. Zhang, K. Liao, J. Gu, Y. Yan, Light-driven heterogeneous reduction of carbon dioxide: photocatalysts and photoelectrodes, *Chem. Rev.* 115 (2015) 12888–12935.
- [20] J. Mao, K. Li, T. Peng, Recent advances in the photocatalytic CO_2 reduction over semiconductors, *Catal. Sci. Technol.* 3 (2013) 2481–2498.
- [21] K. Teramura, Z. Wang, S. Hosokawa, Y. Sakata, T. Tanaka, A doping technique that suppresses undesirable H_2 evolution derived from overall water splitting in the highly selective photocatalytic conversion of CO_2 in and by water, *Chem. Eur. J.* 20 (2014) 9906–9909.
- [22] Z. Wang, K. Teramura, Z. Huang, S. Hosokawa, Y. Sakata, T. Tanaka, Tuning the selectivity toward CO evolution in the photocatalytic conversion of CO_2 with H_2O through the modification of Ag-loaded Ga_2O_3 with a ZnGa_2O_4 layer, *Catal. Sci. Technol.* 6 (2016) 1025–1032.
- [23] Z. Wang, K. Teramura, S. Hosokawa, T. Tanaka, Photocatalytic conversion of CO_2 in water over Ag-modified $\text{La}_2\text{Ti}_2\text{O}_7$, *Appl. Catal. B: Environ.* 163 (2015) 241–247.
- [24] K. Teramura, H. Tatsumi, Z. Wang, S. Hosokawa, T. Tanaka, Photocatalytic conversion of CO_2 by H_2O over Ag-loaded SrO -modified Ta_2O_5 , *Bull. Chem. Soc. Jpn.* 88 (2015) 431–437.
- [25] Z. Wang, K. Teramura, S. Hosokawa, T. Tanaka, Highly efficient photocatalytic conversion of CO_2 into solid CO using H_2O as a reductant over Ag-modified ZnGa_2O_4 , *J. Mater. Chem. A* 3 (2015) 11313–11319.
- [26] Z. Huang, K. Teramura, S. Hosokawa, T. Tanaka, Fabrication of well-shaped $\text{Sr}_2\text{KTa}_5\text{O}_{15}$ nanorods with a tetragonal tungsten bronze structure by a flux method for artificial photosynthesis, *Appl. Catal. B: Environ.* 199 (2016) 272–281.
- [27] S. Iguchi, K. Teramura, S. Hosokawa, T. Tanaka, A ZnTa_2O_6 photocatalyst synthesized via solid state reaction for conversion of CO_2 into CO in water, *Catal. Sci. Technol.* 6 (2016) 4978–4985.
- [28] Y. Hori, H. Wakebe, T. Tsukamoto, O. Koga, Electrocatalytic process of CO selectivity in electrochemical reduction of CO_2 at metal electrodes in aqueous media, *Electrochim. Acta* 39 (1994) 1833–1839.
- [29] M. Yamamoto, T. Yoshida, N. Yamamoto, T. Nomoto, Y. Yamamoto, S. Yagi, H. Yoshida, Photocatalytic reduction of CO_2 with water promoted by Ag clusters in $\text{Ag}/\text{Ga}_2\text{O}_3$ photocatalysts, *J. Mater. Chem. A* 3 (2015) 16810–16816.
- [30] K. Domen, J.N. Kondo, M. Hara, T. Takata, Photo- and mechano-catalytic overall water splitting reactions to form hydrogen and oxygen on heterogeneous catalysts, *Bull. Chem. Soc. Jpn.* 73 (2000) 1307–1331.
- [31] I.-S. Cho, S. Lee, J.H. Noh, D.W. Kim, D.K. Lee, H.S. Jung, D.-W. Kim, K.S. Hong, SrNb_2O_6 nanotubes with enhanced photocatalytic activity, *J. Mater. Chem.* 20 (2010) 3979–3983.
- [32] D. Chen, J. Ye, Selective-synthesis of high-performance single-crystalline $\text{Sr}_2\text{Nb}_2\text{O}_7$ nanoribbon and SrNb_2O_6 nanorod photocatalysts, *Chem. Mater.* 21 (2009) 2327–2333.
- [33] O.C. Compton, C.H. Mullet, S. Chiang, F.E. Osterloh, A building block approach to photochemical water-splitting catalysts based on layered niobate nanosheets, *J. Phys. Chem. C* 112 (2008) 6202–6208.
- [34] Q.-P. Ding, Y.-P. Yuan, X. Xiong, R.-P. Li, H.-B. Huang, Z.-S. Li, T. Yu, Z.-G. Zou, S.-G. Yang, Enhanced photocatalytic water splitting properties of KNbO_3 nanowires synthesized through hydrothermal method, *J. Phys. Chem. C* 112 (2008) 18846–18848.
- [35] H. Shi, Z. Zou, Photophysical and photocatalytic properties of ANbO_3 ($\text{A}=\text{Na, K}$) photocatalysts, *J. Phys. Chem. Solids* 73 (2012) 788–792.
- [36] P. Li, S. Ouyang, Y. Zhang, T. Kako, J. Ye, Surface-coordination-induced selective synthesis of cubic and orthorhombic NaNbO_3 and their photocatalytic properties, *J. Mater. Chem. A* 1 (2013) 1185–1191.
- [37] S. Xie, Y. Wang, Q. Zhang, W. Deng, Y. Wang, SrNb_2O_6 nanoplates as efficient photocatalysts for the preferential reduction of CO_2 in the presence of H_2O , *Chem. Commun.* 51 (2015) 3430–3433.
- [38] Y. Miseki, H. Kato, A. Kudo, Water splitting into H_2 and O_2 over niobate and titanate photocatalysts with (111) plane-type layered perovskite structure, *Energy Environ. Sci.* 2 (2009) 306–314.
- [39] Q. Liu, Y. Zhou, J. Kou, X. Chen, Z. Tian, J. Gao, S. Yan, Z. Zou, High-yield synthesis of ultralong and ultrathin Zn_2GeO_4 nanoribbons toward improved photocatalytic reduction of CO_2 into renewable hydrocarbon fuel, *J. Am. Chem. Soc.* 132 (2010) 14385–14387.
- [40] E. Davis, N. Mott, Conduction in non-crystalline systems V. Conductivity, optical absorption and photoconductivity in amorphous semiconductors, *Philos. Mag.* 22 (1970) 0903–0922.
- [41] E. Wilhelm, R. Battino, R.J. Wilcock, Low-pressure solubility of gases in liquid water, *Chem. Rev.* 77 (1977) 219–262.
- [42] H. Zhong, K. Fujii, Y. Nakano, F. Jin, Effect of CO_2 bubbling into aqueous solutions used for electrochemical reduction of CO_2 for energy conversion and storage, *J. Phys. Chem. C* 119 (2014) 55–61.
- [43] K. Teramura, K. Hori, Y. Terao, Z. Huang, S. Iguchi, Z. Wang, H. Asakura, S. Hosokawa, T. Tanaka, Which is an intermediate species for photocatalytic conversion of CO_2 by H_2O as the electron donor: CO_2 molecule carbonic acid, bicarbonate, or carbonate ions? *J. Phys. Chem. C* 121 (2017) 8711–8721.
- [44] T. Ohno, K. Sarukawa, M. Matsumura, Crystal faces of rutile and anatase TiO_2 particles and their roles in photocatalytic reactions, *N. J. Chem.* 26 (2002) 1167–1170.

Update

Applied Catalysis B: Environmental

Volume 243, Issue , April 2019, Page 804

DOI: <https://doi.org/10.1016/j.apcatb.2017.11.016>



Corrigendum

Corrigendum to “Highly selective photocatalytic conversion of CO₂ by water over Ag-loaded SrNb₂O₆ nanorods” [Appl. catal. B: Environ. 218 (2017) 770–778]



Rui Pang^a, Kentaro Teramura^{a,b,*}, Hiroyuki Asakura^{a,b}, Saburo Hosokawa^{a,b},
Tsunehiro Tanaka^{a,b,*}

Department of Molecular Engineering, Graduate School of Engineering, Kyoto University, Japan
Elements Strategy Initiative for Catalysts & Batteries (ESICB), Kyoto University, Japan

The authors regret < The pH value with NaCl (0.1) as an additive in Table 1 is error, which is shown as 3., the correct pH value should be

3.8. > .

The authors would like to apologise for any inconvenience caused.